Cancer Imaging

RESEARCH ARTICLE Open Access

Magnetic resonance imaging to assess the brain response to fasting in glioblastoma-bearing rats as a model of cancer anorexia

Irene Guadilla[1], Sara González[1], Sebastián Cerdán[1], Blanca Lizarbe[1,2] and Pilar López-Larrubia[1*]

Abstract

Background Global energy balance is a vital process tightly regulated by the brain that frequently becomes dysregulated during the development of cancer. Glioblastoma (GBM) is one of the most investigated malignancies, but its appetite-related disorders, like anorexia/cachexia symptoms, remain poorly understood.

Methods We performed manganese enhanced magnetic resonance imaging (MEMRI) and subsequent diffusion tensor imaging (DTI), in adult male GBM-bearing ($n=13$) or control Wistar rats ($n=12$). A generalized linear model approach was used to assess the effects of fasting in different brain regions involved in the regulation of the global energy metabolism: cortex, hippocampus, hypothalamus and thalamus. The regions were selected on the contralateral side in tumor-bearing animals, and on the left hemisphere in control rats. An additional DTI-only experiment was completed in two additional GBM ($n=5$) or healthy cohorts ($n=6$) to assess the effects of manganese infusion on diffusion measurements.

Results MEMRI results showed lower T_1 values in the cortex (p-value <0.001) and thalamus (p-value <0.05) of the fed ad libitum GBM animals, as compared to the control cohort, consistent with increased Mn^{2+} accumulation. No MEMRI-detectable differences were reported between fed or fasting rats, either in control or in the GBM group. In the $MnCl_2$-infused cohorts, DTI studies showed no mean diffusivity (MD) variations from the fed to the fasted state in any animal cohort. However, the DTI-only set of acquisitions yielded remarkably decreased MD values after fasting only in the healthy control rats (p-value <0.001), and in all regions, but thalamus, of GBM compared to control animals in the fed state (p-value <0.01). Fractional anisotropy (FA) decreased in tumor-bearing rats due to the infiltrate nature of the tumor, which was detected in both diffusion sets, with (p-value <0.01) and without Mn^{2+} administration (p-value <0.001).

Conclusions Our results revealed that an altered physiological brain response to fasting occurred in hunger related regions in GBM animals, detectable with DTI, but not with MEMRI acquisitions. Furthermore, the present results showed that Mn^{2+} induces neurotoxic inflammation, which interferes with diffusion MRI to detect appetite-induced responses through MD changes.

Keywords Diffusion tensor imaging, Manganese enhanced MRI, Glioblastoma, Cancer anorexia, Fasting paradigm

*Correspondence:
Pilar López-Larrubia
plopez@iib.uam.es
Full list of author information is available at the end of the article

Background

Global energy balance is a complex systemic response that involves the coordination of numerous organs, including the brain. A plethora of dedicated neuronal pathways located in different cerebral regions coordinates the homeostatic adjustment between food intake and energy expenditure [1]. This delicate homeostatic equilibrium is found to be perturbed in many neurological disorders, such as in patients with malignant tumors, who usually develop anorexia (loss of appetite), a major component of cancer cachexia [2]. In fact, anorexia/cachexia syndrome is one of the most common causes of death among cancer patients and, in advanced stages, can reach approximately 80% of cases [3]. Although malignant gliomas are among the most investigated tumors, the mechanisms underlying their devastating appetite-related consequences remain poorly understood. Indeed, although anorexia and body weight loss are specific signs of cachexia in glioma patients, the symptoms of glioma associated with cachexia have received little attention [4, 5]. It is also important to note that fatigue, as another important symptom of cachexia, has a prevalence in glioma patients ranging from 39 to 77% [6].

Magnetic resonance imaging (MRI) is used routinely to obtain morphological and functional information of the brain. In particular, diffusion weighted imaging (DWI) and diffusion tensor imaging (DTI) can characterize cerebral microstructure [7, 8]. Their usage already extends to a wide range of cerebral pathologies, including oncological diseases, ischemic episodes, neurodegeneration, mental disorders and brain trauma [9, 10]. Complementary information on cerebral activation may be gathered from functional neuroimaging perspectives [11], including diffusion functional MRI [12], or manganese enhanced magnetic resonance imaging (MEMRI) [13].

Briefly, diffusion functional studies are based on MRI detection of changes in translational motion of water molecules resulting from activation-induced ionic transferring and associated neurocellular swelling/shrinking events. Such effects can be evaluated by quantifying the alterations in the diffusion coefficients, like mean diffusivity (MD) and fractional anisotropy (FA), using mono-exponential [14, 15], bi-exponential, or even tri-exponential models that can separate the diffusion regimes of water molecules into different compartments [16, 17]. Previous research demonstrated that diffusion MRI protocols are able to detect fasting-induced alterations in the brains of mice, rats and humans [18], suggesting that they could provide valuable information about the effects of tumor growth on brain regulation of global energy homeostasis.

MEMRI, on the other hand, can be used as a preclinical functional imaging methodology in animal models and it is based on the systemic administration of a manganese ion (Mn^{2+}) solution to reveal areas of neural activity. This is achieved by tracking the Mn^{2+} accumulation in neural cells during neurotransmission, which occurs by its competition with the calcium ion (Ca^{2+}) in voltage-gated Ca^{2+} channels [19, 20]. Mn^{2+} is a paramagnetic cation that induces spin–lattice relaxation time (T_1) shortening proportional to its concentration accumulation, thus revealing areas of neuronal activation with brighter enhancement in T_1 weighted (T_1W) images [21]. Mn^{2+} accumulates in the neuronal endoplasmic reticulum, is transported through axonal tracts and reaches the presynaptic membrane. It is then released into the synaptic cleft and finally uptaken by the postsynaptic neuron [22]. This fact allows the generation of functional maps of neural pathways acting as a trans-synaptic, tract-tracing methodology, identifying perturbations that can be associated with neuropathologies [23]. In the rodent brain, studies using MEMRI with systemic infusions of $MnCl_2$ detected altered hypothalamic neuronal activity associated with fasting [24, 25], and the corresponding effects in genetically obese mice [26]. However, the use of MEMRI is limited to preclinical studies due to its associated neurotoxicity [27]. Notably, although the potential of MEMRI and DTI in the assessment of functional anatomy has been explored [28, 29], the compatibility of both methodologies in the evaluation of brain responses to a stimulus have not yet been investigated to our knowledge.

We hypothesized that brain activity underlying physiological responses to hunger might be disrupted or suppressed in glioblastoma (GBM) bearing animals and be detected by DTI and MEMRI methodologies. This must probably occur in specific brain areas involved in the regulation of food intake, such as the cortex, hippocampus, hypothalamus and thalamus [30]. The abnormal imaging findings at specific hunger-related regions in GBM-bearing animals may represent underlying alterations in neuronal activity and suggest the contribution of GBM to cachexia in GBM patients. The ability to assess it could make an important contribution to the monitoring of therapies aimed at improving appetite disorders in cancer patients.

Materials and methods

Animals and experimental design

All experimental procedures were approved by the Ethic Committees of the Biomedical Research Institute "Alberto Sols", the Spanish National Research Council (CSIC) and the Community of Madrid (PROEX 047/18) and follow the national (R.D.53/2013) and European Community guidelines (2010/62/UE) for care and management of experimental animals. The design and

reporting adhered to the ARRIVE guidelines [31]. Rats were housed in the animal premises of our institution (Reg. No. ES280790000188) and cared for by specialized personnel.

Male adult Wistar rats (own production) ($n=25$, 220–250 g, body weight, b.w.) were randomly separated in two main groups: control ($n=12$) and tumor-bearing animals ($n=13$). For the GBM model group, rat glioma C6 cells (ATCC® CCL-107 TM) were used after growing in Dulbecco's Modified Eagle Medium (DMEM) modified with 10% FBS, streptomycin sulfate (0.12 mL/400 mL of DMEM), and bencilpeniciline (0.14 mL/400 mL of DMEM). Rats were given inhalatory anesthesia inside a box (2–2.5% isoflurane/oxygen) and then placed on a stereotaxic device (Model 900LS Small Animal Stereotaxic Instrument, Kopf Instruments®) where 10^5 cells in 10 µl of DMEM medium were injected in the right caudate nucleus using bregma as skull landmark: 0.35 mm right-lateral and 0.55 mm ventral [32]. Animals received buprenorphine (0.03 mg/kg, b.w.) subcutaneously as analgesic right after the surgery and the following two days. Tumor growth was followed with anatomical spin–spin relaxation time weighted (T_2W) MR images, acquired every 3 days, starting 10 days after the intracranial injection of the glioma cells. When the gliomas were in an advanced stage, MRI studies were performed on the animals to assess brain response to food deprivation.

Control and GBM animals were subdivided into two groups to be assessed under fed ad libitum (6 control and 6 GBM) or fasting conditions after 16 h of food deprivation (6 control and 7 GBM) (Supplementary Fig. 1A). A solution of $MnCl_2$ (100 mM, pH = 7.4) was injected subcutaneously by using an infusion pump and a cannula tubing placed in the abdominal area at a dosage of 1 mmol/kg b.w. and a flow rate of 0.1 mL/min. Mn^{2+} infusions were performed 24 h prior to MRI acquisitionsunder inhalational anesthesia [20].

Additional animals ($n=11$, 220–250 g, b.w.) were randomly divided in two new cohorts: control ($n=6$) and GBM ($n=5$). They were used to evaluate DTI parameters under feeding and, 24 h later, under fasting conditions in the absence of Mn^{2+} solution administration (Supplementary Fig. 1B).

Magnetic resonance imaging studies

Image acquisitions were carried out in a Bruker BioSpec® 7 T system (Bruker Biospin, Ettlingen, DE), 16 cm bore, with a 90 mm gradient insert of 360 mT/m and a 40 mm quadrature volume resonator, interfaced with an Avance III radiofrequency console and running ParaVision 5.1 software.

Anesthetized animals (induced with 2–2.5% and maintained with 1–1.5% isoflurane/oxygen) were placed in a methyl methacrylate rat-holder of the MRI system and restrained with a bite-bar attached to a nose mask and a small piece of tape over the head and attached to the animal's bedding. Anatomical images acquired to monitor tumor development consisted of a RARE fast spin-echo T_2W acquisition, with the following parameters: repetition time (TR) = 3000 ms, echo time (TE) = 44 ms, averages (Av) = 2, RARE factor = 8, 10 continuous slices with 1.5 mm of thickness in axial orientation, matrix data (Mtx) = 256×256 and 0.14×0.14 mm^2/pixel in plane resolution.

When the tumors reached an advanced stage (volume > 100 mm^3, coincident with high state of physical deterioration), DTI and MEMRI evaluations were performed 24 h after Mn^{2+} infusion to achieve the greatest effect on T_1W image signal intensity. Each day, two animals were studied at the same time interval. To minimize bias, animals were randomly selected independently of experimental cohort (GBM or control) and feeding status (fed or fasted). To avoid circadian variations in neuronal activity [33], the imaging sessions always began at 8 a.m.. Prior to the imaging session, all rats were weighed on an electronic balance (0.1 g accuracy), and blood glucose levels were measured with a standard glucometer from a drop of blood from the tail tip. Once in the rat holder, a circulating warm water blanket was placed under the animal to maintain a stable body temperature during imaging acquisition. A small animal monitoring device (Model 1025, SA Instruments, Inc. NY) was used to follow the physiological status of the rats by measuring rectal temperature with an electronic thermometer and respiratory rate with a pneumatic pillow placed in the abdominal region. The respiratory rate was maintained between 40 and 60 breaths per minute by regulating the concentration of the anesthetic administered (1–1.5% isoflurane/oxygen).

The MRI protocol designed to evaluate the brain response to hunger in rats included two sets of acquisitions. A non-gated DTI study was performed employing the following features and parameters: TR = 2500 ms, TE = 43 ms, Av = 5, 5 slices in axial orientation with slice thickness = 1.5 mm and no-gap, Mtx = 128×128, 0.25×0.25 mm^2/pixel in-plane resolution, single-shot echo-planar imaging (ss-EPI), diffusion gradients applied in 6 non-coplanar and non-collinear directions, gradient diffusion separation (Δ) = 20 ms, gradient diffusion duration (δ) = 4 ms, and b values of 0, 200 and 1000 s/mm^2. Then, the MEMRI evaluation was carried out by employing a saturation-recovery experiment with a RARE sequence at variable TR to generate T_1 maps with the following parameters: 7 TRs (150, 200, 400, 800, 1600, 3500 and 6000 ms), TE = 12.6 ms, Av = 1, 5 slices in axial orientation with slice thickness = 1.5 mm and no-gap,

Mtx = 128 × 128 and 0.25 × 0.25 mm^2/pixel in-plane resolution. The total acquisition time of the study was 45 min for each animal in the MEMRI + DTI study and 20 min in rats in the DTI-only evaluation.

Image processing and data analysis

Data from MRI studies were processed with MyMap-Analyzer, a homemade script developed in MATLAB (R2010b, the MathWorks Inc., Natick, MA) to generate the parametric images. MRI datasets from the DTI acquisitions were fit in a pixel-by-pixel base to a mono-exponential model to generate mean diffusivity (MD) and fractional anisotropy (FA) maps [34].

MRI signals of T_1W images were fitted in a pixel-by-pixel base to Eq. 1 to obtain the corresponding T_1 maps.

$$S_{(TR)} = S_0(1 - e^{(-TR/T_1)}) \quad (1)$$

where $S_{(TR)}$ is the signal intensity at a specific TR value, S_0 is the signal intensity at a hypothetical TR = 0, and TR are each one of the 7 TR values employed (from 150 to 6000 ms).

In all cases, images were computed without any additional pre-processing procedures. As a measure of the goodness-of-fit to the estimated linear (for T_1 maps) and multiple (for DTI) regression equations, only pixels with a value of $R^2 > 0.75$ were included in the subsequent analysis. Four regions of interest (ROIs) related to the brain's response to hunger [35, 36] -cortex, hippocampus, hypothalamus and thalamus- were assessed on the contralateral side in tumor-bearing animals in order to avoid imaging effects related to the GBM itself [37]. The same four ROIs were defined in the left hemisphere in control rats. ROIs containing 20–22 pixels (approximately 2 mm^3) were manually selected on T_2W images with an anatomical rat brain atlas as a guide [38], and overlaid on the parametric maps. For the selection of the ROIs, the same central slice was always used, in which the four regions can be unequivocally identified. Finally, the parameters were measured with ImageJ software (National Institutes of Health, Bethesda, MD, USA, ImageJ) and subsequently individual data from all pixels of the ROIs were statistically evaluated. Image processing and analysis was performed blinded to fed/fasted conditions.

Statistical analysis

Statistical analyses to assess body weight and blood glucose levels differences in the four groups (control fed, control fasted, tumor-bearing fed, tumor-bearing fasted) were performed by corresponding unpaired multiple t-tests (fed vs fasted and control vs tumor-bearing) corrected with the Holm-Sidak method using GraphPad Prism software (GraphPad Software, La Jolla, CA, USA). The MRI parametric data were statistically analyzed using the IBM SPSS package (IBM SPSS Statistics for Windows, Version 25.0, Armonk, NY, IBM Corp.). Comparison of ROI data derived from parametric maps of animals in different experimental conditions was performed using a generalized linear model (GzLM) with generalized estimating equations (GEE). In this model, the dependent variables (MD, FA and T_1) were related to the independent factors (control or tumor) and condition (fed or fasted). Data are presented as mean ± one standard deviation. In all cases, only *p*-values smaller than 0.05 were considered to be statistically significant.

Results

Physiological results

Overnight fasting resulted in a significant decrease of body weight (measured 24 h apart) in healthy but not in tumor-bearing animals: control fed (241.7 ± 7.6 g) vs control fasted (230.9 ± 8.4 g) had a *p*-value = 0.05, while tumor fed (281.6 ± 30.0 g) vs tumor fasted (270.9 ± 30.2 g) had a *p*-value = 0.49. In any case, a similar percentage of weight lost was achieved for both control and GBM cohorts (Fig. 1A). Glucose concentration decreased with fasting in both groups, although it reached statistical significance in the control group (Fig. 1B).

Effects of fasting in tumor-bearing animals assessed with MRI

MEMRI and DTI studies were performed in control and tumor-bearing rats under both ad libitum feeding and fasting conditions. Representative images (T_2W, T_1W, and diffusion images) of a rat with GBM obtained in a MRI session are presented in Supplementary Fig. 2. The ROIs of the different regions investigated (Fig. 2A), were manually selected in T_2W images and then exported to the corresponding parametric images.

Representative T_1 maps of Mn^{2+}-infused animals (Fig. 2B) for each state (control or tumor-bearing) and feeding condition (fed or 16 h-fasted), and the corresponding data are summarized in Fig. 2C-F and Supplementary Table 1, respectively. Statistical analysis of the data with GEE using feeding state, condition and region as independent factors revealed a significant effect of region (*p*-value < 0.001) and the product "state *x* condition *x* region" (*p*-value < 0.001). Pairwise analysis revealed that in the ad libitum feeding condition, control animals had significantly higher T_1 values than tumor-bearing rats in both cortical (*p*-value = 0.001) and thalamic (*p*-value = 0.019) regions (Fig. 2C and F, respectively), but not in the hippocampus or hypothalamus (Fig. 2D and E, respectively). Comparison of T_1 data for fasted animals did not reach statistical significance in any region.

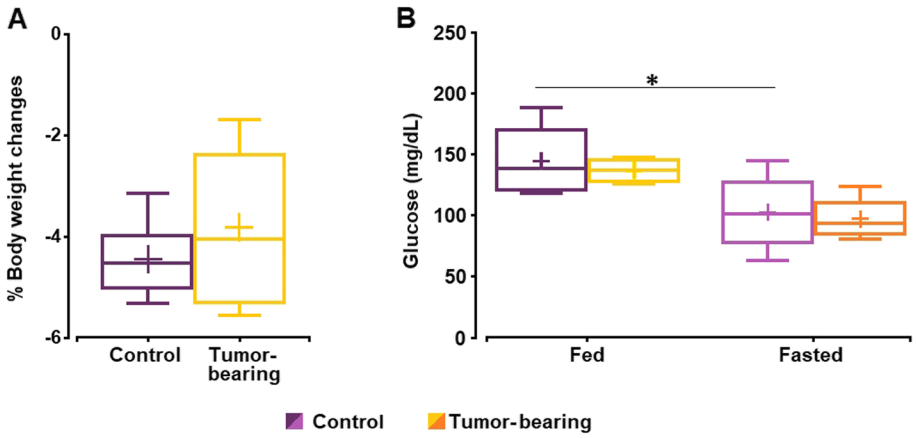

Fig. 1 Decrease in body weight and blood glucose level in control and GBM rats under fed or fasted conditions. **A** Body weight changes after 16 h of food deprivation. **B** Blood glucose levels before the MRI session in fed and fasted conditions. In each box-plot, the central mark indicates the median, the cross mark the mean, and the bottom and top edges refer to the 25-th and 75-th percentiles, respectively. The upper and lower limits of the box extend to the most extreme data points not considered outliers (* p-value < 0.05)

No significant differences were detected when comparing ROIs between feeding conditions in either control or GBM-bearing rats (Supplementary Table 1).

The results of DTI studies performed during the MEMRI imaging session are presented in Fig. 3 with illustrative MD (Fig. 3A) and FA (Fig. 3B) maps of control and rats with GBM under both feeding and fasting conditions. The corresponding data are also shown in Supplementary Table 2. The GEE approach of the MD values obtained revealed a significant effect of the feeding state (p-value = 0.022), region (p-value < 0.001) and the product "state x condition x region" (p-value < 0.001). Pairwise comparisons of this parameter between controls and tumor-bearing animals in the fed measurements depicted no significant differences in any region. In the fasting condition, only the thalamus presented significantly lower MD values in rats with GBM compared to control animals (Fig. 3C). GEE assessment of the FA data revealed a significant effect of the state (p-value = 0.002), region (p-value < 0.001) and the product "state x condition x region" (p-value < 0.001). FA values were significantly lower in the cortex, hippocampus and thalamus of tumor-bearing rats in the fed condition compared to control (p-value < 0.01 in the three ROIs). Under fasting the cortex and hippocampus of GBM animals showed significantly lower values (p-value < 0.05 in the two ROIs) (Fig. 3D).

Finally, none of the DTI parameters present significant differences between feeding conditions in any region, when evaluated separately, either in the control or in the GBM cohorts (Supplementary Table 2).

To test whether the absence of DTI changes with fasting or with tumor presence was related to the $MnCl_2$ infusion, DTI studies were acquired on a new set of animal cohorts (6 control and 5 GBM) under the same experimental protocol (fed ad libitum and after 16 h of food deprivation), without $MnCl_2$ administration. Representative maps of non-Mn^{2+} infused animals are shown as examples for each parameter (MD and FA), pathological state (control and tumor) and feeding status (fed and fasted) (Fig. 4A and B). The corresponding MD and FA results are presented (Fig. 4C and D, respectively) and tabulated (Supplementary Table 3). Statistical evaluation of the MD values exposed the significant effect of state (p-value = 0.001), condition (p-value < 0.001), region (p-value < 0.001), and the product "state x condition x region" (p-value < 0.001). In the fed condition, MD in tumor-bearing rats was significantly lower than in control animals in the cortex, hippocampus and hypothalamus, while under fasting, significance was maintained only in hippocampus (Fig. 4C). Furthermore, food deprivation in control animals induced a decrease in MD, reaching statistical significance (p-value < 0.001) in the cortex, hippocampus and thalamus, but this event did not occur in GBM rats (Fig. 4C). The GEE approach also revealed that FA values were significantly affected by state, region and the product "state x condition x region" (p-value < 0.001 for all cases). Data showed significantly lower FA in the tumor group than in the control cohort in the cortex, hippocampus and thalamus, in both fed and fasting condition (p-value < 0.001) (Fig. 4D).

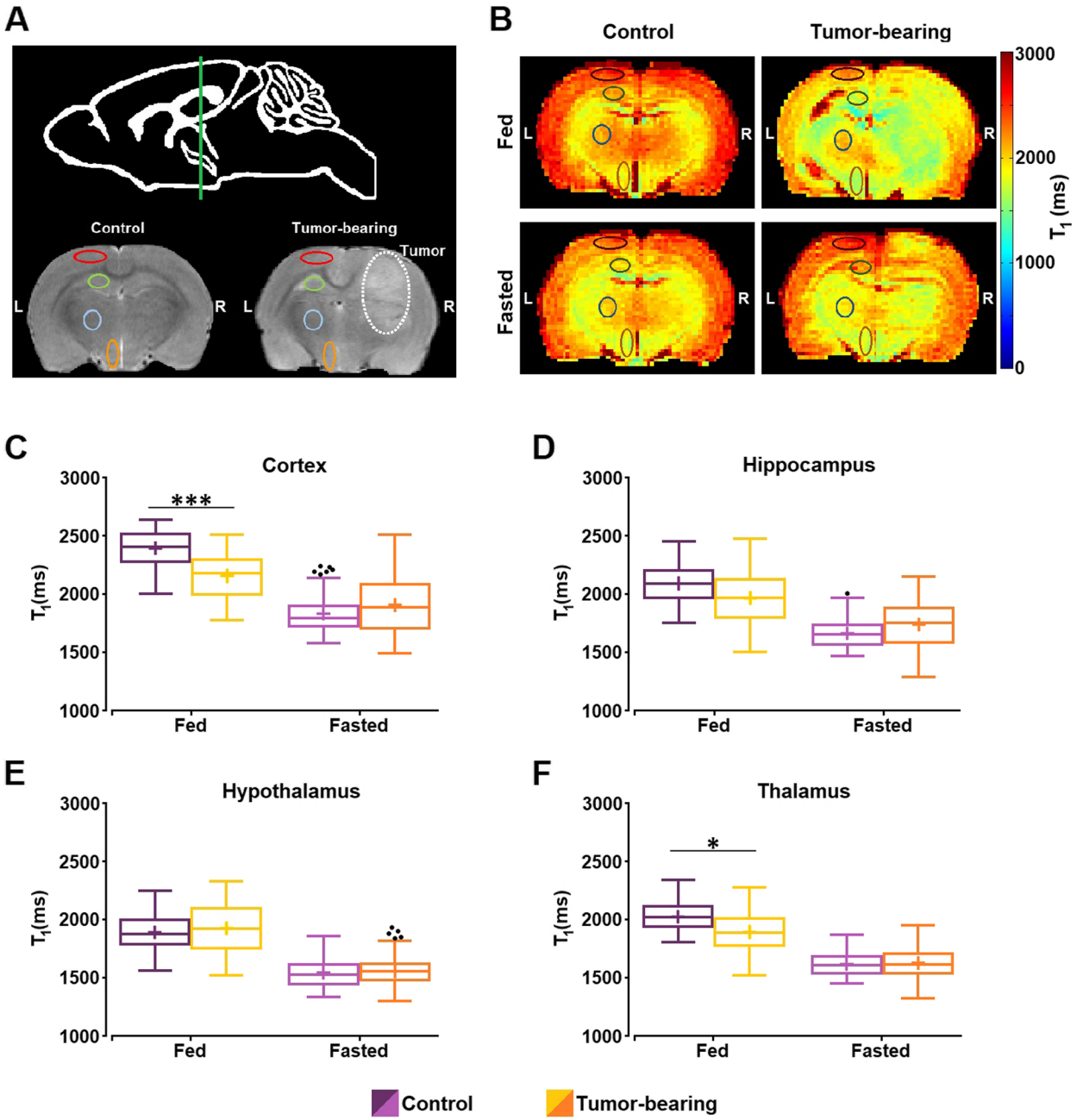

Fig. 2 MEMRI of control and GBM rats, 24 h after Mn^{2+} administration, under fed or fasted conditions. **A** Anatomical location of the slice selected, including the perimeters of the investigated ROIs in the left contralateral hemisphere: cortex (red), hippocampus (green), thalamus (blue) and hypothalamus (orange). **B** Representative T_1 maps of a control and a tumor-bearing animal, 24 h after Mn^{2+} administration, under fed and fasted conditions. The ROIs (cortex, hippocampus, hypothalamus and thalamus) are outlined in the maps. **C-F** Boxplots of T_1 values from the different ROIs investigated, in control and GBM rats, under fed and fasted conditions. Box plots are represented as indicated in Fig. 1. Outliers are plotted individually using the '•' symbol. (* p-value < 0.05, *** p-value < 0.001)

Discussion

MRI techniques have evolved into very powerful tools to non-invasively characterize the anatomy and function of the normal brain and its pathologies. In particular, diffusion imaging and MEMRI methods allow for the assessment of physiological processes directly related to neural activation and cerebral microarchitecture. Previous research has used diffusion techniques or MEMRI to investigate brain mechanisms related to appetite and hunger [25, 35, 39], but to our knowledge, the effects of

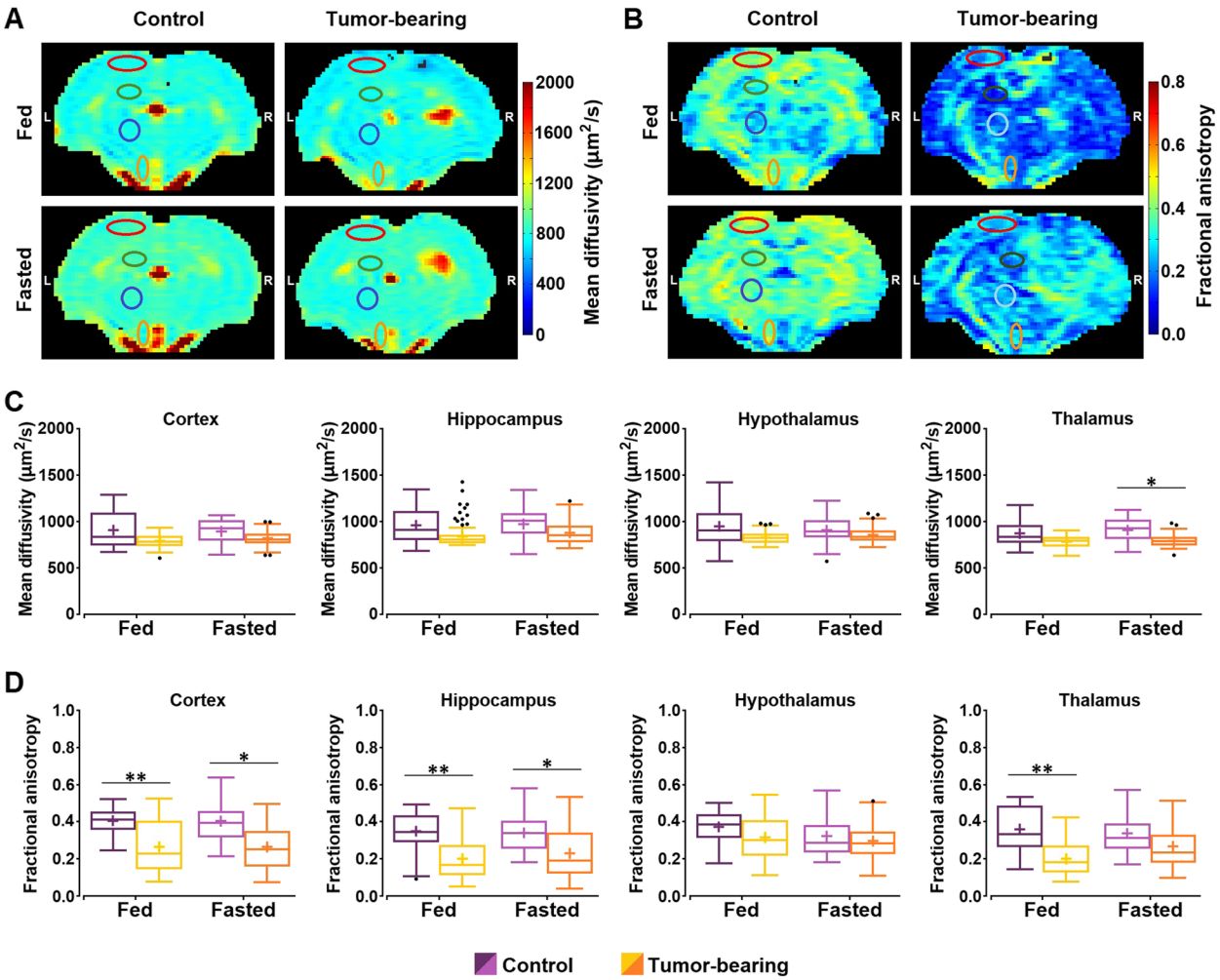

Fig. 3 Mean diffusivity and fractional anisotropy in the brain of control and GBM rats under fed or fasted conditions 24 h after Mn^{2+} administration. **A**, **B** Representative parametric maps of mean diffusivity (MD) and fractional anisotropy (FA) of a control and a tumor-bearing rat, under fed and fasted conditions, respectively. The ROIs (cortex, hippocampus, hypothalamus and thalamus) are outlined in the maps. **C**, **D** Boxplots of the MD and FA values, respectively, from the different regions investigated (cortex, hippocampus, hypothalamus and thalamus) in control cohort and tumor-bearing rats under fed and fasted conditions. Box plots are represented as indicated in Fig. 1. Outliers are plotted individually using the '•' symbol. (* p-value < 0.05, ** p-value < 0.01)

a brain tumor development on such feeding mechanisms had not previously been addressed. Moreover, previous works describe the use of MEMRI and DTI in vivo and ex vivo to evaluate the brain integrity, mainly the white matter, in different neuropathological conditions [40, 41]. Although previous work has used both MRI approaches in the same animals and imaging sessions to assess the axonal uptake and transport optic nerve [42], the use of both methodologies in the assessment of brain responses to feeding-related stimuli is lacking. In this work, we combine and compare DTI and MEMRI approaches to investigate brain responses to starvation in a rat model of glioblastoma by evaluating related imaging parameters in feeding and fasting states.

Different brain regions are involved in the regulation of the global energy metabolism [30, 43], several of which are investigated in this work. The hypothalamus is the most significant due to the high number of orexigenic and anorexigenic cells [44]. The cortex acts as the primary gustatory region that processes the odor and texture of food and perceived pleasantness. The hippocampus has a high concentration of receptors for ghrelin, insulin and leptin hormones which are related to appetite regulation [45]. The thalamus, in turn, receives inputs from appetite-related hypothalamic nuclei [36]. Thus, these regions were investigated in the in vivo MRI study presented here.

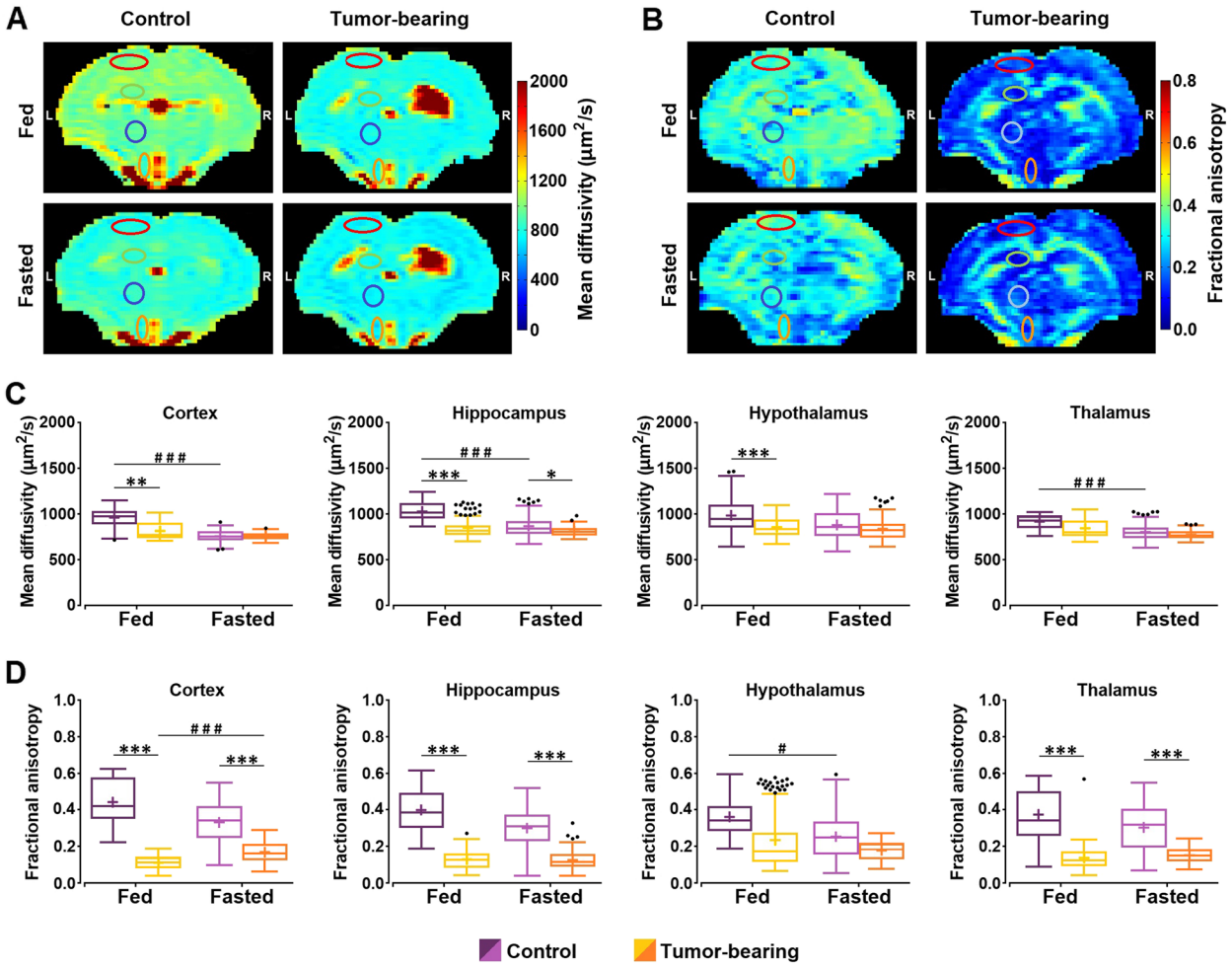

Fig. 4 Mean diffusivity and fractional anisotropy in the brain of control and GBM rats under fed or fasted conditions without $Mn.^{2+}$ administration. **A**, **B** Representative parametric maps of mean diffusivity (MD) and fractional anisotropy (FA) of a control and a tumor-bearing rat, under fed and fasted conditions, respectively. The ROIs (cortex, hippocampus, hypothalamus and thalamus) are outlined in the maps. **C**, **D** Boxplots of the MD and FA values, respectively, from the different regions investigated (cortex, hippocampus, hypothalamus and thalamus) in control cohort and tumor-bearing rats under fed and fasted conditions. Box plots are represented as indicated in Fig. 1. Outliers are plotted individually using the '•' symbol. (*/# p-value < 0.05, ** p-value < 0.01, ***/### p-value < 0.001)

In our work, the physiological data showed that all animals experienced a decrease in body weight due to food deprivation with similar percentages of reduction in the control and GBM cohorts. Such weight loss, however, only reached statistical significance in the control animals. We suspect that the greater interindividual variability in the b.w. evolution of GBM-bearing animals after de C6 cells injection may be undermining the significance of this tendency. Similarly, all animals showed lower fasting glucose levels, but the difference was significant in control rats, suggesting an abnormal response to fasting in rats with glioma. Taken together, both results point to a potentially altered regulation of food intake and glycemic response to food deprivation on GBM rats, the latter deserving to be evaluated in future studies.

MEMRI methodologies have been widely used to map neuronal pathways, define morphological boundaries and study connectivity in structural and brain activation imaging studies [21, 46, 47]. Mn^{2+} enters and accumulates in excitable cells through voltage-gated Ca^{2+} channels. Since the increase in T_1 signal is directly related to Mn^{2+} accumulation in an activity dependent manner, MEMRI allows the identification and quantification of neural activity. In the present study, T_1 values obtained from $MnCl_2$-infused rats were significantly lower in the cortex and thalamus of GBM rats fed ad libitum than controls under the same feeding condition. The decrease

in T_1 reflects a higher Mn^{2+} accumulation in the corresponding regions of GBM animals, thus revealing increased neuronal activation. These results are consistent with previous studies reporting abnormal neuronal excitability, and progressive desynchronization of neuronal activity, in contralateral brain regions of glioma-bearing mice [48]. In addition, several studies have shown that the infiltrative nature of GBM can induce neuronal hyperexcitability through an anomalous increase in the synaptic glutamate release and a decrease in GABAergic inhibitory signals [49, 50].

After 16 h of food deprivation, our MEMRI approach did not identify significant changes in T_1, either in control or GBM fasted rats. Previous studies using MEMRI reported increased neuronal activity in the hypothalamic nuclei during a similar overnight fasting period in mice [25], or after 24 h of food deprivation, as well as in rats with dehydration-induced anorexia [24]. The first study, however, was methodologically different from the present one, as it involved a 2-h $MnCl_2$ infusion performed simultaneously with MR acquisitions, instead of the current protocol which used a faster Mn^{2+} administration (approx. 25 min) 24 h prior to scanning. In addition, the increased signal in the arcuate nucleus (ARC) was observed to decay 1 h after the beginning of administration, revealing a relatively rapid diffusion process of Mn^{2+} out of the ARC into the remaining hypothalamic nuclei and potentially into other hunger-regulating structures. Furthermore, in both studies the authors imaged at higher magnetic fields (9.4 and 14.1 T) that allowed for sub-hypothalamic regionalization, which is less feasible in our 7 T system. Since the hypothalamic nuclei that comprise the hypothalamus are known to exhibit different activation patterns, it remains possible that our hypothalamic ROI averaged dissimilar responses, for example activation or inhibition, resulting in undetectable net changes.

Unexpectedly, the DTI studies performed 24 h after $MnCl_2$ administration failed to detect any significant change in diffusion parameters with fasting. We have previously reported significant changes in brain diffusion coefficients in healthy mice, rats and humans after food deprivation, reflecting the orexigenic activity-induced cellular swelling responses to hunger [18, 35]. In the present study, we suspect that the Mn^{2+} administration interferes with the diffusion-detected brain response to starvation. Significantly lower FA values were found in the cortex, hippocampus and thalamus of fed tumor-bearing rats as compared to controls, and in the cortex and hippocampus of the same group under fasting. This suggests a loss of brain parenchymal integrity in animals with tumor, such as those detected in rat glioma models [51, 52] and in patients diagnosed with high-grade glioma [53, 54]. Thus, this decrease in the FA values in the GBM rats may involve a number of additional effects including increased cell density, lack of fiber integrity, cancer cell infiltration processes, and/or microvascular alterations Future research with microvascular and tractography dedicated MRI approaches and histological studies, will need to address the physiological origin of the FA changes reported here.

Mn^{2+} is known to trigger in the brain a neurotoxicity response [27], which involves neuro-inflammation [55]. Previous studies have also reported that Mn^{2+} can induce microglial activation by triggering the secretion of proinflammatory factors like TNFα, iNOS and IL-1β [56]. The release of these proinflammatory factors usually affects the integrity of the blood–brain barrier causing water extravasation and the appearance of vasogenic edema. Notably, an increase of the extracellular water content in the brain tissue is detected in diffusion MRI studies as an increase in the diffusion coefficients [10]. As mentioned above, according to previous investigations, food deprivation is expected to cause activity-induced cellular swelling, which is detected as a local decrease of MD in the regions involved. The present results do not show this finding, likely due to an opposing and overlapping neuroinflammatory effect. This result can derive from Mn^{2+} neurotoxicity that may be obscuring the normal brain response to fasting in Mn^{2+} infused animals. Although the timing of the manganese-related proinflammatory response is not clearly described our results suggest that this effect is likely to occur as soon as the cation accumulates in cells through the Ca^{2+} channels, and Mn^{2+} levels are known to increase significantly in the brain 24 h after administration [57].

To investigate whether the effects of Mn^{2+} actually interfered with the determination of water diffusion in the brain, we performed DTI studies in two new cohorts of rats not previously infused with $MnCl_2$. Our data revealed that the control cohort showed a significant decrease in MD values after 16 h of food deprivation, as expected previously [18]. However, tumor-bearing rats presented comparable MD coefficients under fed and fasting conditions, suggesting that the normal brain response to fasting is altered in the GBM animals. Taken together, our data suggest that glioma induces important alterations in the brain, preventing a normal cerebral response to fasting, and probably contributing to the development of eating disorders as those described in brain cancer patients [5]. Indeed, abnormal cerebral responses and tumor-related neurocognitive dysfunction are widely reported circumstances in glioma patients [58–60], which may underlie loss of appetite in brain cancer patients, paving the way to cachexia [61].

Comparisons in non-Mn^{2+} infused between tumor and control cohorts under the same feeding conditions revealed significantly lower MD values in the cortex, hippocampus and hypothalamus of fed GBM rats, and in the hippocampus of fasted GBM animals. In this regard, increased cellularity in high-grade gliomas is reported to induce a decrease in water diffusion as the tumor grows [62, 63], and the return of the apparent diffusion coefficient to higher values with cancer treatment may be used as an early detection marker of the therapeutic success [62]. Thus, the decrease in MD observed in the contralateral region of rats with GBM may indicate long-range cell proliferation processes due to the infiltrative nature of the tumor, or even long-range compression effects derived from tumor growth. Both possibilities are well supported by changes in FA values, even in $MnCl_2$-infused animals. Finally, pairwise fed vs. fasted comparisons in each independent cohort resulted in significantly fasting-reduced FA values in the hypothalamus of the control rats, and fasting-augmented FA values in the cortex of the tumor-bearing animals. Reduced FA values in the hypothalamic region of the control animals may represent the microstructural consequence of neurocellular swelling events associated with fasting. These swelling events physiologically resemble cytotoxic edema, a circumstance reported to be closely related to FA [64], although the molecular mechanisms remain to be elucidated. In GBM rats, the regional increases in FA probably again reflect compression effects arising from the presence of the tumor. As in the study with Mn^{2+} infused animals, FA values of non-Mn^{2+} infused animals were significantly lower in the cortex, hippocampus and thalamus of GBM rats under both fed and fasting conditions. This finding suggests once again that the decrease in FA in the contralateral hemisphere is likely related to the infiltrative nature of the tumor, the effects of compression, and the resulting microstructural changes.

Importantly, our study has several limitations. First, the number of animals per group may seem low. However, the total number of animals aligns with the bioethical considerations and a respectful use of laboratory animals. In addition, the sample size of the experimental groups in our work is very similar to those used in analogous preclinical studies with rats as models of brain pathologies. Second, the use of improved DTI sequences could allow us to segment nuclei in the hypothalamus and find alterations that were not seen in our current data. And third, histological studies could be performed to assess the brain alterations detected with DTI.

Conclusion

The present study evaluated two complementary MRI techniques that provide functional information -DTI and MEMRI- in the assessment of brain responses to fasting in a glioblastoma model in rats. MEMRI studies identified increased neuronal excitability due to the presence of the tumor, although they could not detect the effects of overnight fasting. Moreover, our data revealed that the neurotoxic effects of Mn^2 significantly interferes with the use of diffusion imaging methodologies. Although the molecular mechanisms underlying Mn^{2+} interference in diffusion-detected brain activation deserve further investigation, it is clear that these perturbances hinder the use of MEMRI and diffusion methodologies in the same MRI session.

In addition, DTI studies revealed microstructural alterations in the contralateral region of tumor-bearing animals. DTI in absence of Mn^{2+} did identify neurocellular swelling related to the fasting condition in healthy rats. However, in animals with advanced stage GBM, no changes were detected, suggesting impairment of hunger responses.

In summary, both MEMRI and DTI results suggest that tumor-induced changes in the brain alter the network necessary for proper regulation of energy balance, which provides further insight into the understanding of cancer-associated eating disorders and progression to cancer-associated anorexia and cachexia.

Abbreviations

δ	Gradient diffusion duration
Δ	Gradient diffusion separation
ARC	Arcuate nucleus
Ca^{2+}	Calcium ion
DTI	Diffusion tensor imaging
DWI	Diffusion weighted imaging
FA	Fractional anisotropy
GBM	Glioblastoma multiforme
GEE	Generalized estimating equations
GzLM	Generalized linear model
MD	Mean diffusivity
MEMRI	Manganese enhanced magnetic resonance imaging
Mn^{2+}	Manganese ion
MRI	Magnetic resonance imaging
Mtx	Matrix data
ROIs	Regions of interest
TE	Echo time
TR	Repetition time

Supplementary Information

The online version contains supplementary material available at https://doi.org/10.1186/s40644-023-00553-y.

Additional file 1: Supplementary Figure 1. Experimental design. **A** Animals included in the control and tumor-bearing cohorts, submitted to the infusion of a 100 mM $MnCl_2$ solution 24 h prior the MRI session, that included MEMRI and DTI evaluations, under fed or fasted conditions. **B** Animals included in the control and tumor-bearing cohorts, in fed and

fasted conditions, subjected only to DTI studies. The same animals were studied, one day apart, under the two-feeding status. **Supplementary Figure 2.** Representative images of an MRI session. The panels show the five slices acquired in a rat with GBM: **A** T_2W images; **B** T_1W images, from a MEMRI study, at TR = 400 ms; **C** diffusion images, from a DTI study, acquired in one direction at b = 200 s/mm^2; **D** diffusion images from the same DTI study and direction, but acquired at b = 1000 s/mm^2. The tumors are manually outlined with a white line. **Supplementary Table 1.** Mean value and standard deviation (SD) of T_1 values 24h after $MnCl_2$ infusion, for each cohort of rats, region, state and feeding condition. No statistical differences were found in the pairwise comparison of fed vs fasted animals for every brain region**. Supplementary Table 2.** Mean value and standard deviation (SD) of MD and FA, 24h after $MnCl_2$ infusion, for each cohort, region, state and feeding condition. No statistical differences were found in the pairwise comparison of fed vs fasted animals for every brain region. **Supplementary Table 3.** Mean value and standard deviation (SD) of MD and FA of each cohort, region, state and feeding condition. *p*-values correspond to the comparison fed vs. fasted animals in the absence of Mn^{2+} infusion.

Acknowledgements
IG was supported by predoctoral fellowship BES-2015-075202, BL held a senior postdoctoral contract from CSIC, and SC and PLL were CSIC staff investigators. Authors are indebted to Mrs. Maria J. Guillén for continuous technical support and proficient animal handling. The CSIC MRI Facility is a central research resource of the Instituto de Investigaciones Biomédicas "Alberto Sols", running under fee for service conditions and maintained by institutional funds.

Authors' contributions
Irene Guadilla: methodology, software, formal analysis, investigation, writing—original draft. Sara González: methodology, software, formal analysis. Sebastián Cerdán: writing—review & editing, funding acquisition. Blanca Lizarbe: validation, investigation, resources, writing—original draft; writing—review & editing, supervision, funding acquisition. Pilar López-Larrubia: conceptualization, methodology, validation, investigation, resources, writing—original draft; writing—review & editing, supervision, funding acquisition, project administration. The author(s) read and approved the final manuscript.

Funding
Open Access funding provided thanks to the CRUE-SIC agreement with Springer Nature. This work was supported in part by grants PID2021-122528OB-I00 (MICINN/AEI/FEDER, UE) to PLL, S2017/BMD-3688 (CM/FEDER/FSE, UE) to SC and PLL, and PID2021-126888OA-I00 (MICINN/AEI/FEDER, UE) to BL. IG was supported by predoctoral fellowship BES-2015–075202.

Availability of data and materials
The data presented in this study are available on request from the corresponding author due to the need for a formal data sharing agreement.

Declarations

Ethics approval and consent to participate
All experimental procedures were approved by the Ethic Committees of the Biomedical Research Institute "Alberto Sols", the Spanish National Research Council (CSIC) and the Community of Madrid (PROEX 047/18), and follow the national (R.D.53/2013) and European Community guidelines (2010/62/UE) for care and management of experimental animals.

Consent for publication
Not applicable.

Competing interests
The authors declare that the research was conducted in the absence of any commercial or financial relationships that could be construed as a potential conflict of interest.

Author details
[1]Biomedical Magnetic Resonance Group, Instituto de Investigaciones Biomédicas Alberto Sols, CSIC-UAM, C/ Arturo Duperier 4, 28029 Madrid, Spain. [2]Departamento de Bioquímica, Universidad Autónoma de Madrid, 28029 Madrid, Spain.

Received: 15 November 2022 Accepted: 3 April 2023
Published online: 10 April 2023

References

1. Schwartz MW, Morton GJ. Keeping hunger at bay. Nature. 2002;418:595–7.
2. Ezeoke CC, Morley JE. Pathophysiology of anorexia in the cancer cachexia syndrome: pathophysiology of anorexia. J Cachexia Sarcopenia Muscle. 2015;6:287–302.
3. von Haehling S, Anker SD. Prevalence, incidence and clinical impact of cachexia: facts and numbers-update 2014. J Cachexia Sarcopenia Muscle. 2014;5:261–3.
4. Cui P, Shao W, Huang C, Wu C-J, Jiang B, Lin D. Metabolic derangements of skeletal muscle from a murine model of glioma cachexia. Skeletal Muscle. 2019;9:3.
5. Griffith JL, Hochberg FH. Anorexia and weight loss in glioma patients. Psychosomatics. 1988;29:335–7.
6. van Coevorden-van Loon EMP, Coomans MB, Heijenbrok-Kal MH, Ribbers GM, van den Bent MJ. Fatigue in patients with low grade glioma: systematic evaluation of assessment and prevalence. J Neurooncol. 2017;133:237–46.
7. Martín Noguerol T, Martínez Barbero JP. Advanced diffusion MRI and biomarkers in the central nervous system: a new approach. Radiología (English Edition). 2017;59:273–85.
8. Huisman TAGM. Diffusion-weighted and diffusion tensor imaging of the brain, made easy. Cancer Imaging. 2010;10:S163–71.
9. Sundgren PC, Dong Q, Gómez-Hassan D, Mukherji SK, Maly P, Welsh R. Diffusion tensor imaging of the brain: review of clinical applications. Neuroradiology. 2004;46:339–50.
10. Drake-Pérez M, Boto J, Fitsiori A, Lovblad K, Vargas MI. Clinical applications of diffusion weighted imaging in neuroradiology. Insights Imaging. 2018;9:535–47.
11. Seeck M, Spinelli L, Gotman J, Lopes da Silva FH. Combination of brain functional imaging techniques. Schomer DL, Lopes da Silva FH, editors. Oxford University Press; 2017. Available from: https://academic.oup.com/book/35515/chapter/305265692 [cited 24 Mar 2023].
12. Le Bihan D, Urayama SI, Aso T, Hanakawa T, Fukuyama H. Direct and fast detection of neuronal activation in the human brain with diffusion MRI. Proc Natl Acad Sci. 2006;103:8263–8.
13. Koretsky AP, Silva AC. Manganese-enhanced magnetic resonance imaging (MEMRI). NMR Biomed. 2004;17:527–31.
14. Mayo CD, Garcia-Barrera MA, Mazerolle EL, Ritchie LJ, Fisk JD, Gawryluk JR, et al. Relationship between DTI metrics and cognitive function in Alzheimer's disease. Front Aging Neurosci. 2019;10:436.
15. Abe Y, Tsurugizawa T, Le Bihan D. Water diffusion closely reveals neural activity status in rat brain loci affected by anesthesia. PLoS Biol. 2017;15:e2001494 Rushworth M, editor.
16. Zeng Q, Shi F, Zhang J, Ling C, Dong F, Jiang B. A modified tri-exponential model for multi-b-value diffusion-weighted imaging: a method to detect the strictly diffusion-limited compartment in brain. Front Neurosci. 2018;12:102.
17. Le Bihan D. Diffusion, confusion and functional MRI. Neuroimage. 2012;62:1131–6.
18. Lizarbe B, Benítez A, Sánchez-Montañés M, Lago-Fernandez L, Garcia-Martin M, López-Larrubia P, et al. Imaging hypothalamic activity using diffusion weighted magnetic resonance imaging in the mouse and human brain. Neuroimage. 2012;64:448–57.
19. Fa Z, Zhang P, Wu W, Wang Z, Huang F, Yang L, et al. Functional mapping of rat brain activation following rTMS using activity-induced manganese-dependent contrast. Neurol Res. 2011;33:563–71.
20. Silva AC, Lee JH, Aoki I, Koretsky AP. Manganese-enhanced magnetic resonance imaging (MEMRI): methodological and practical considerations. NMR Biomed. 2004;17:532–43.

21. Yang J, Li Q. Manganese-enhanced magnetic resonance imaging: application in central nervous system diseases. Front Neurol. 2020;11:143–143.
22. Malheiros JM, Paiva FF, Longo BM, Hamani C, Covolan L. Manganese-enhanced MRI: biological applications in neuroscience. Front Neurol. 2015;6:161–161.
23. Cloyd RA, Koren SA, Abisambra JF. Manganese-enhanced magnetic resonance imaging: overview and central nervous system applications with a focus on neurodegeneration. Front Aging Neurosci. 2018;10:403.
24. Just N, Gruetter R. Detection of neuronal activity and metabolism in a model of dehydration-induced anorexia in rats at 14.1 T using manganese-enhanced MRI and 1 H MRS: Manganese-Enhanced MRI Of anorexic rats. NMR Biomed. 2011;24:1326–36.
25. Kuo Y-T, Herlihy AH, So P-W, Bell JD. Manganese-enhanced magnetic resonance imaging (MEMRI) without compromise of the blood–brain barrier detects hypothalamic neuronal activityin vivo. NMR Biomed. 2006;19:1028–34.
26. Delgado TC, Violante IR, Nieto-Charques L, Cerdán S. Neuroglial metabolic compartmentation underlying leptin deficiency in the obese *ob/ob* mice as detected by magnetic resonance imaging and spectroscopy methods. J Cereb Blood Flow Metab. 2011;31:2257–66.
27. Dobson AW, Erikson KM, Aschner M. Manganese neurotoxicity. Ann N Y Acad Sci. 2004;1012:115–28.
28. Obenaus A, Jacobs RE. Magnetic resonance imaging of functional anatomy: use for small animal epilepsy models. Epilepsia. 2007;48:11–7.
29. Chan KC, Cheng JS, Fan S, Zhou IY, Yang J, Wu EX. In vivo evaluation of retinal and callosal projections in early postnatal development and plasticity using manganese-enhanced MRI and diffusion tensor imaging. Neuroimage. 2012;59:2274–83.
30. Caron A, Richard D. Neuronal systems and circuits involved in the control of food intake and adaptive thermogenesis: neural control of energy balance. Ann NY Acad Sci. 2017;1391:35–53.
31. Kilkenny C, Browne W, Cuthill I, Emerson M, Altman D. Improving bioscience research reporting: the ARRIVE guidelines for reporting animal research. J Pharmacol Pharmacother. 2010;1:94.
32. García-Martín ML, Hérigault G, Rémy C, Farion R, Ballesteros P, Coles JA, et al. Mapping extracellular pH in rat brain gliomas in vivo by 1H magnetic resonance spectroscopic imaging: comparison with maps of metabolites. Cancer Res. 2001;61:6524–31.
33. Akana SF, Strack AM, Hanson ES, Dallman MF. Regulation of activity in the hypothalamo-pituitary-adrenal axis is integral to a larger hypothalamic system that determines caloric flow. Endocrinology. 1994;135:1125–34.
34. Le Bihan D, Mangin J-F, Poupon C, Clark CA, Pappata S, Molko N, et al. Diffusion tensor imaging: Concepts and applications. J Magn Reson Imaging. 2001;13:534–46.
35. Guadilla I, Lizarbe B, Barrios L, Cerdán S, López-Larrubia P. Integrative analysis of physiological responses to high fat feeding with diffusion tensor images and neurochemical profiles of the mouse brain. Int J Obes. 2021;45:1203–14.
36. Kahathuduwa CN, Boyd LA, Davis T, O'Boyle M, Binks M. Brain regions involved in ingestive behavior and related psychological constructs in people undergoing calorie restriction. Appetite. 2016;107:348–61.
37. Montgomery MK, Kim SH, Dovas A, Zhao HT, Goldberg AR, Xu W, et al. Glioma-induced alterations in neuronal activity and neurovascular coupling during disease progression. Cell Rep. 2020;31:107500.
38. Paxinos G, Watson C. Paxino's and Watson's The rat brain in stereotaxic coordinates. 7th ed. Amsterdam; Boston: Elsevier/AP, Academic Press is an imprint of Elsevier; 2014.
39. Jensen T, Kiersgaard M, Sørensen D, Mikkelsen L. Fasting of mice: a review. Lab Anim. 2013;47:225–40.
40. Martirosyan NL, Turner GH, Kaufman J, Patel AA, Belykh E, Kalani MYS, et al. Manganese-enhanced MRI offers correlation with severity of spinal cord injury in experimental models. TONIJ. 2016;10:139–47.
41. Nishioka C, Liang H-F, Ong S, Sun S-W. Axonal transport impairment and its relationship with diffusion tensor imaging metrics of a murine model of p301L tau induced tauopathy. Neuroscience. 2022;498:144–54.
42. Lin T-H, Chiang C-W, Trinkaus K, Spees WM, Sun P, Song S-K. Manganese-enhanced MRI (MEMRI) via topical loading of Mn^{2+} significantly impairs mouse visual acuity: a comparison with intravitreal injection: topical Mn^{2+} loading impairs visual function. NMR Biomed. 2014;27:390–8.
43. Rui L. Brain regulation of energy balance and body weight. Rev Endocr Metab Disord. 2013;14:387–407.
44. Dietrich MO, Horvath TL. Hypothalamic control of energy balance: insights into the role of synaptic plasticity. Trends Neurosci. 2013;36:65–73.
45. Davidson TL, Kanoski SE, Schier LA, Clegg DJ, Benoit SC. A potential role for the hippocampus in energy intake and body weight regulation. Curr Opin Pharmacol. 2007;7:613–6.
46. Xiao Z, Tang Z, Wu L, Feng X, Sun X, Tang W, et al. Manganese-enhanced magnetic resonance imaging in the whole visual pathway: chemical identification and neurotoxic changes. Acta Radiol. 2019;60:1653–62.
47. Lu H, Xi Z-X, Gitajn L, Rea W, Yang Y, Stein EA. Cocaine-induced brain activation detected by dynamic manganese-enhanced magnetic resonance imaging (MEMRI). Proc Natl Acad Sci USA. 2007;104:2489–94.
48. Montgomery MK, Kim SH, Dovas A, Patel K, Mela A, Humala N, et al. Glioma-induced alterations in neuronal activity and neurovascular coupling during disease progression. Cell Rep. 2020;31:107500.
49. Campbell SL, Buckingham SC, Sontheimer H. Human glioma cells induce hyperexcitability in cortical networks. Epilepsia. 2012;53:1360–70.
50. Buckingham SC, Campbell SL, Haas BR, Montana V, Robel S, Ogunrinu T, et al. Glutamate release by primary brain tumors induces epileptic activity. Nat Med. 2011;17:1269–74.
51. Li X-Y, Chen J-Q, Xu Y-K, Han X-J. The relationship between fractional anisotropy value and tumor microarchitecture in late-stage rat glioma. Asian Pac J Trop Med. 2017;10:607–11.
52. Wang S, Zhou J. Diffusion tensor magnetic resonance imaging of rat glioma models: a correlation study of MR imaging and histology. J Comput Assist Tomogr. 2012;36:739–44.
53. Verburg N, Koopman T, Yaqub MM, Hoekstra OS, Lammertsma AA, Barkhof F, et al. Improved detection of diffuse glioma infiltration with imaging combinations: a diagnostic accuracy study. Neuro Oncol. 2020;22:412–22.
54. Kallenberg K, Goldmann T, Menke J, Strik H, Bock HC, Mohr A, et al. Abnormalities in the normal appearing white matter of the cerebral hemisphere contralateral to a malignant brain tumor detected by diffusion tensor imaging. Folia Neuropathol. 2014;52:226–33.
55. Tjalkens RB, Popichak KA, Kirkley KA. Inflammatory activation of microglia and astrocytes in manganese neurotoxicity. Adv Neurobiol. 2017;18:159–81.
56. Liu M, Cai T, Zhao F, Zheng G, Wang Q, Chen Y, et al. Effect of microglia activation on dopaminergic neuronal injury induced by manganese, and its possible mechanism. Neurotox Res. 2009;16:42–9.
57. Dinamene S, Camila BM, Tavares de Almeida I, Davis Randall L, Luisa MM, Vanda A, et al. Evaluation of neurobehavioral and neuroinflammatory end-points in the post-exposure period in rats sub-acutely exposed to manganese. Toxicology. 2013;314:95–9.
58. Anderson SW, Damasio H, Tranel D. Neuropsychological impairments associated with lesions caused by tumor or stroke. Arch Neurol. 1990;47:397–405.
59. Hahn CA, Dunn RH, Logue PE, King JH, Edwards CL, Halperin EC. Prospective study of neuropsychologic testing and quality-of-life assessment of adults with primary malignant brain tumors. Int J Radiat Oncol Biol Phys. 2003;55:992–9.
60. Weitzner MA, Meyers CA, Byrne K. Psychosocial functioning and quality of life in patients with primary brain tumors. J Neurosurg. 1996;84:29–34.
61. Solheim TS, Blum D, Fayers PM, Hjermstad MJ, Stene GB, Strasser F, et al. Weight loss, appetite loss and food intake in cancer patients with cancer cachexia: Three peas in a pod? – analysis from a multicenter cross sectional study. Acta Oncol. 2014;53:539–46.
62. Roberts TA, Hyare H, Agliardi G, Hipwell B, d'Esposito A, Ianus A, et al. Noninvasive diffusion magnetic resonance imaging of brain tumour cell size for the early detection of therapeutic response. Sci Rep. 2020;10:9223.
63. Baehring JM, Bi WL, Bannykh S, Piepmeier JM, Fulbright RK. Diffusion MRI in the early diagnosis of malignant glioma. J Neurooncol. 2007;82:221–5.
64. Lee JK, Liu D, Jiang D, Kulikowicz E, Tekes A, Liu P, et al. Fractional anisotropy from diffusion tensor imaging correlates with acute astrocyte and myelin swelling in neonatal swine models of excitotoxic and hypoxic-ischemic brain injury. J Comp Neurol. 2021;529:2750–70. https://doi.org/10.1002/cne.25121.

Publisher's Note